

Antireflective design of Si-based photovoltaics via biomimicking structures on black butterfly scales

Zhongjia Huang^{a,b,*}, Xinying Shi^{c,*}, Gang Wang^{a,b}, Petri Leukkunen^b, Marko Huttula^b, Wei Cao^{b,a}

^a School of Mechanical and Automotive Engineering, Anhui Polytechnic University, Wuhu, 241000, China.

^b Nano and Molecular Systems Research Unit, University of Oulu, P.O. Box 3000, FIN-90014, Oulu, Finland.

^c School of Physics and Electronic Engineering, Jiangsu Normal University, Xuzhou, 221116, China.

* Corresponding authors at School of Mechanical and Automotive Engineering, Anhui Polytechnic University, Wuhu, 241000, China (Z. Huang); School of Physics and Electronic Engineering, Jiangsu Normal University, Xuzhou, 221116, China (X. Shi).

E-mail addresses: hzj@ahpu.edu.cn (Z. Huang), xshi@jsnu.edu.cn (X. Shi).

Abstract

The naturally evolved sunlight harvesters are not limited to foliage. Animals also harvest sunlight for light-heat conversion. A typical antireflective and light-trapping scheme has been well demonstrated on thin butterfly scales where solar energy is converted to heat besides being diffracted for surface coloration. Biomimicking scale structures offers a unique route to enhance light harvesting efficiencies happening on manmade solar cells. Herein, we performed a computational investigation of using microstructures on black butterflies for solar cell efficiency enhancement. Scale microstructures were obtained from nine species of black butterflies and employed as coating structures in numerical models built on Si-slabs. Introducing butterfly wing structures not only reduces the light reflection and transmittance but also increases the light absorption within Si-slabs. Surface reflection was decreased down to 10%, and the

short-circuit current was increased by 66% correspondingly. An antireflection design strategy is given and hoped to benefit light harvesting in Si-based solar cells eventually.

Keywords: Butterfly wing scale; Optical property; Reflectance; FDTD simulation

1. Introduction

The way of utilizing solar energy is one of the most straightforward routes to solve energy crisis for human's sustainability (Lewis, 2016). Direct light-electricity conversion heavily relies on Si-based photovoltaics (PV) which dominates global solar cell market due to the cost-efficiency balances and industrial readiness (Conibeer et al., 2006; Hong et al., 2014), despite upcoming novel materials and their technical progresses (Fujishima et al., 2009; Paudel and Yan, 2013). However, the Si slab surface reflects more than 35% incident solar radiances (Ikhmayies, 2018), causing significant loss of light input. Thus, reducing the surface reflectance becomes crucial to enhance light harvesting efficiency for Si-based solar cells.

So far, many works have been dedicated to introducing manmade antireflective (AR) features on Si-slabs (Li et al., 2018; Yue et al., 2013). One typical technique is texturing Si solar cells with pyramid structures at micrometer scales (Ju et al., 2016; Sopori et al., 1999). Pyramid textures can reduce light reflection and enhance light absorption as well as the path length of light through solar cells (Fonash 2014; Manzoor et al., 2020). Therefore light trapping can be enhanced by such pyramid textures. The flat slab can be patterned with Si nano-arrays subjected to multi-steps of etching and surface

reconstruction. As a result, the ‘black silicon’ reduces light reflection and realizes a high quantum efficiency of 22% in the lab conditions (Savin et al., 2015; Duan et al., 2018). Directly coating Si surface with AR layers has been also widely applied in recent years (Lelièvre et al., 2019; Li et al., 2018; Schmidt et al., 2012). Among various AR coatings, silicon nitride ($\text{SiN}_x\text{:H}$) has been a popular coating material (Schmidt and Aberle, 1999; Wu et al., 2015). It benefits solar cells from its characteristics of anti-reflection and surface passivation (Hofstetter et al., 2007). Through dedicated encapsulation, multi-layered coverage can diminish reflections among layered interfaces, and the final acceptance of light can be increased on the Si unit (Ko et al., 2011; Dullweber et al., 2013; Li, et al., 2019). For example, Ko et al. (2011) prepared $\text{SiN}_x\text{:H}$ double layers on silicon wafers. The refractive indices of $\text{SiN}_x\text{:H}$ double layers were 1.9 and 2.3 for the top and bottom layers, respectively. With optimum thickness of 60 and 20 nm for the top and bottom layers, such $\text{SiN}_x\text{:H}/\text{Si}/\text{SiN}_x\text{:H}$ structure presented an average reflectance of 24.86% in the wavelength range of 300 – 500 nm. Compared with the multi-staged methods, a straighter one-step coating strategy has been developed to guide light wave propagation inside of the layered medium. Very typical master structures were copied from plant foliage surfaces (Huang et al., 2015; Huang et al., 2018) for the AR purposes. Quantum efficiency (QE) has been enhanced in the real conditions where incident light reaches the surface at small angles (Liu et al., 2016).

Switching light guider to trapper can also facilitate harvesting efficiency. Unique surface structures offer a capability to alter the original optical performances of the

substrates, e.g., light reflection and absorption, structural color effect (Shi et al., 2019), and optical haze (Huang et al., 2015). A well-known light trapping structure is the black butterfly scale (Han et al., 2012; Zhan et al., 2019). A recent work has shown microstructures of scales (Siddique et al., 2017) also helps QE increase. Therein, light wave is trapped by the microstructure generated from the butterfly scale. Consequently, more solar irradiance will be captured by the cell unit. Despite such a progress, it is noticed that the light trapping structures also facilitate light-heat conversion. The scales on dark color wings typically act as light-absorbers to fast elevate body temperature or get ice removed in extreme cases (Wasserthal, 1975). This means part of light is converted into heat instead of being transmitted. In addition, vast varieties of black butterflies and dark color given by the wings may also lead to differences in photon acceptor performances. A thorough evaluation is needed to investigate light-trapping structures as surface patterns on Si-based photovoltaics.

In this paper, we presented an antireflection design strategy by using surface structures of butterfly scales to benefit Si-based solar cells. Nano- and micrometer level morphologies were obtained from nine different butterflies and employed as prototypical structures on Si photovoltaics in numerical simulations. Detailed relationships between scale nanostructures and their influences on optical behaviors were computationally studied. It is found that introducing butterfly wing structures not only reduced the light reflection and transmittance but also increased the light absorption. As a result, the light harvesting on Si-based photovoltaics was elevated. Besides presenting an antireflective

design strategy for high-performance solar cells, this work is hoped to provide biomimicry inspirations for future optical device designs.

2. Methods

2.1 Butterfly types

In this study, the investigated butterfly wing scales were obtained from butterfly species of *Ornithoptera priamus*, *Aglais io*, *Tirumala limniace*, *Polyura athamas*, *Graphium doson*, *Graphium sarpedon*, *Papilio protenor cramer*, *Papilio helenus*, and *Papilio xuthus*. Since butterfly wings of pure black are not common, the region-of-interests (ROI) were black regions of the aforementioned butterfly types.

2.2 Characterizations

Digital photographs of the butterfly wings were taken by a Canon EOS 350D digital camera, and the microstructures of the scales were investigated through a scanning electron microscope (SEM, ZEISS Sigma). To facilitate the SEM characterizations, the black regions of the wings were cut and glued to the SEM holder with silver glue, and then were deposited by gold layers. For optical measurements, the black wing scale regions were cut into 10×10mm squares. Those square pieces were fixed onto optical glass slides with glue coated on sample edges. The central regions of the square samples were aligned on the optical path during measurements. Optical properties such as surface reflectance, transmission and absorption of the wings were measured through a Shimadzu UV-2600 Spectrophotometer equipped with an integral sphere.

2.3 Computational details

The silicon was selected as modelling material to replicate the butterfly wing structures and evaluate their photovoltaic properties. The photovoltaic cells are constructed on 1.2 μm thick Si slabs. The optical simulations were carried out with Lumerical software through finite-difference-time-domain (FDTD) methods. The three-dimensional models were constructed following the butterfly wing structures. To facilitate the computation, a unit structure of the models was selected for simulation. The planar dimensions (X and Y) were computed following periodic boundary condition while complete absorption boundary condition was employed in Z dimension. Plane wave light was applied as the light source, and the simulation time was primarily set as 10,000 femtoseconds (fs). The light wavelength covers a spectral range from 300 nm to 800 nm. Finally, the short-circuit current was calculated by the Solar Generation associated within the FDTD software. The open-circuit voltage and fill factor were not calculated. During the simulation, the top cladding of the structure is assumed to be air. Any native surface oxide is neglected. The silicon substrate is layered on top of a Si ideal material that does not include bulk and surface recombination effects. Electrical contacts were not taken into consideration during the simulation. Various butterfly wings were studied to figure out the effect of wing structures on optical performances. For each wing model, the hole size was altered to evaluate the relationships between hole sizes and optical behaviors. After the simulation, the computed data were transferred from time domain to frequency domain by discrete Fourier transform method. The simulated spectra were generated.

3. Results and discussions

3.1 Microstructures of butterfly wings

Surface structures in micro- or nanometer scale strongly interact with visible light and thus have great effect on optical properties. The morphology characterizations demonstrate that the microstructures of the black regions of butterfly wings are composed by V-type gullies and various hole features between two adjacent ridges. The holes show the shapes of cover scales on the wings. According to the hole features, the wings are classified into four types: type-I (V-gullies without holes), type-II (V-gullies with one line of holes), type-III (V-gullies with two lines of holes) and type-IV (V-gullies with three lines of holes).

Fig. 1 shows the photos of *Ornithoptera priamus* and the morphology of its wing surface. The wing scale has a type-I structure and is labelled as IA in this paper. V-shape gullies are parallel which were formed by two ridges. The bottom of the ridges has a length of 800 nm and 200 nm away from adjacent ones. The ridges therefore have a periodic spacing of 1 μm . The V-gullies are on top of net-shape structures.

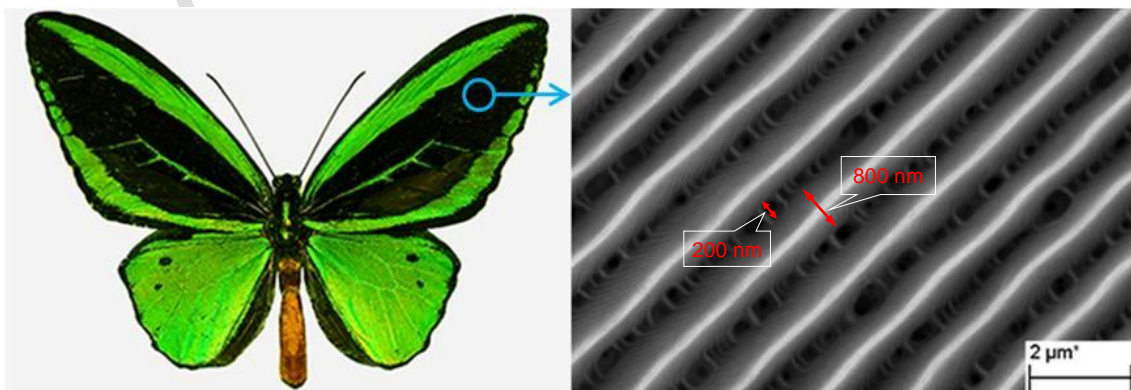
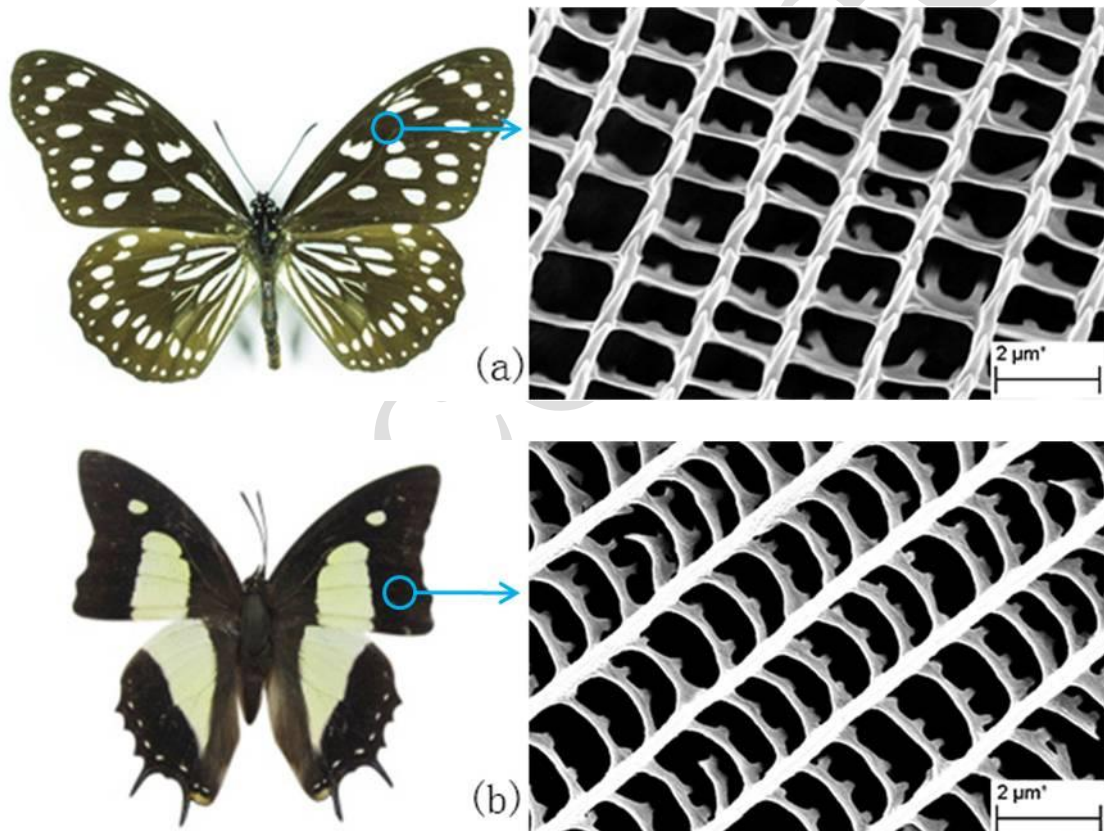


Fig. 1. The optical photos of *Ornithoptera priamus* and the SEM image of the black region

of its wing surface.

The wings of *Tirumala limniace* (IIA, Fig. 2a), *Polyura athamas* (IIB, Fig. 2b) and *Aglais io* (IIC, Fig. 2c) demonstrate the type-II structure. There is one line of rectangular holes between adjacent ridges. The different butterfly species could be identified by period lengths (L) of ridges and hole widths (W). The morphologies in Fig. 2 show three structures where $L = 1.7 \mu\text{m}$, $2 \mu\text{m}$, $2 \mu\text{m}$ and $W = 700 \text{ nm}$, 880 nm , 600 nm of the above three butterfly wings.



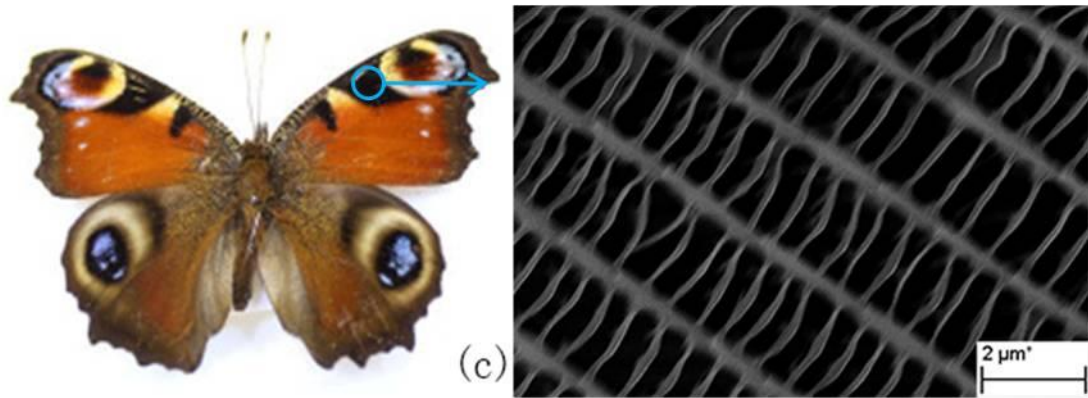
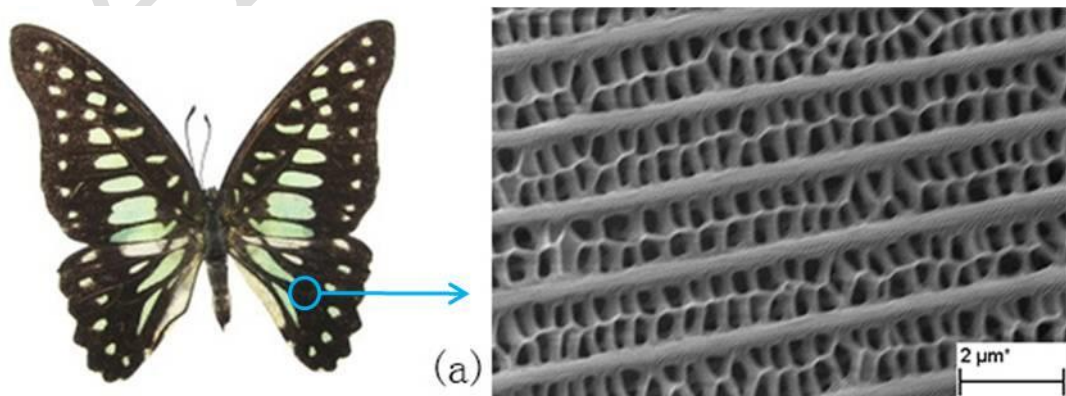


Fig. 2. The photos and SEM images of type-II butterfly wings. (a) *Tirumala limniace*, (b) *Polyura athamas*, (c) *Aglais io*.

The butterfly wings of *Graphium doson* and *Graphium sarpedon* are shown in Fig. 3 (type-III). There are two lines of holes between adjacent ridges. As for the *Graphium doson* butterfly (IIIA, Fig. 3a), the ridges have a periodic length of $1.75\ \mu\text{m}$ and a length of $800\ \text{nm}$ for each hole. The hole width is shorter ($500\ \text{nm}$) than its length. Fig. 3b shows the *Graphium sarpedon* wing (IIIB) has a ridge periodic length of $1.5\ \mu\text{m}$, hole length of $700\ \text{nm}$ and width of $500\ \text{nm}$.



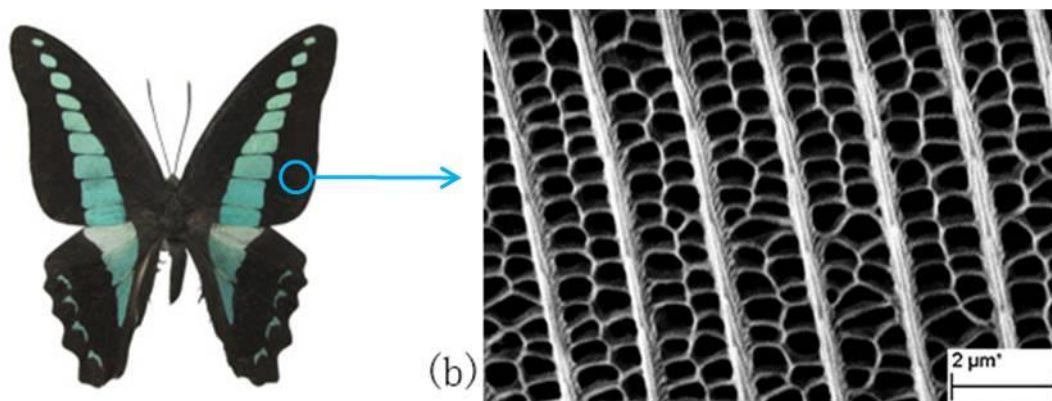


Fig. 3. The photos and SEM images of type-III butterfly wings. (a) *Graphium doson*, (b) *Graphium sarpedon*.

The type-IV wing structures are shown in Fig. 4. For the three species, there are three lines of holes arranged within adjacent ridges. The hole shapes are no longer rectangular but trapezoid-like for those next to a ridge and polygonal for those in the middle line. *Papilio protenor cramer* (IVA, Fig. 4a) has a wing structure with a periodic ridge length of $2.5\ \mu\text{m}$, hole size of $740\ \text{nm} \times 650\ \text{nm}$ for those next to a ridge and average diameters of $700\ \text{nm}$ for those in the middle. In Fig. 4b, *Papilio helenus* wings (IVB) show a periodic ridge length of $2.4\ \mu\text{m}$ filled with $800\ \text{nm} \times 400\ \text{nm}$ holes next to ridges and holes with diameters of $450\ \text{nm}$ between two trapezoidal ones. For *Papilio xuthus* wings (IVC) in Fig. 4c, the ridges repeated by $2.5\ \mu\text{m}$, and the holes next to ridges are $650\ \text{nm} \times 450\ \text{nm}$ and the ones in the middle have average diameters of $550\ \text{nm}$. Among the three types of wings that contain holes, the average hole sizes become smaller with the increasing lines of holes within one gully.

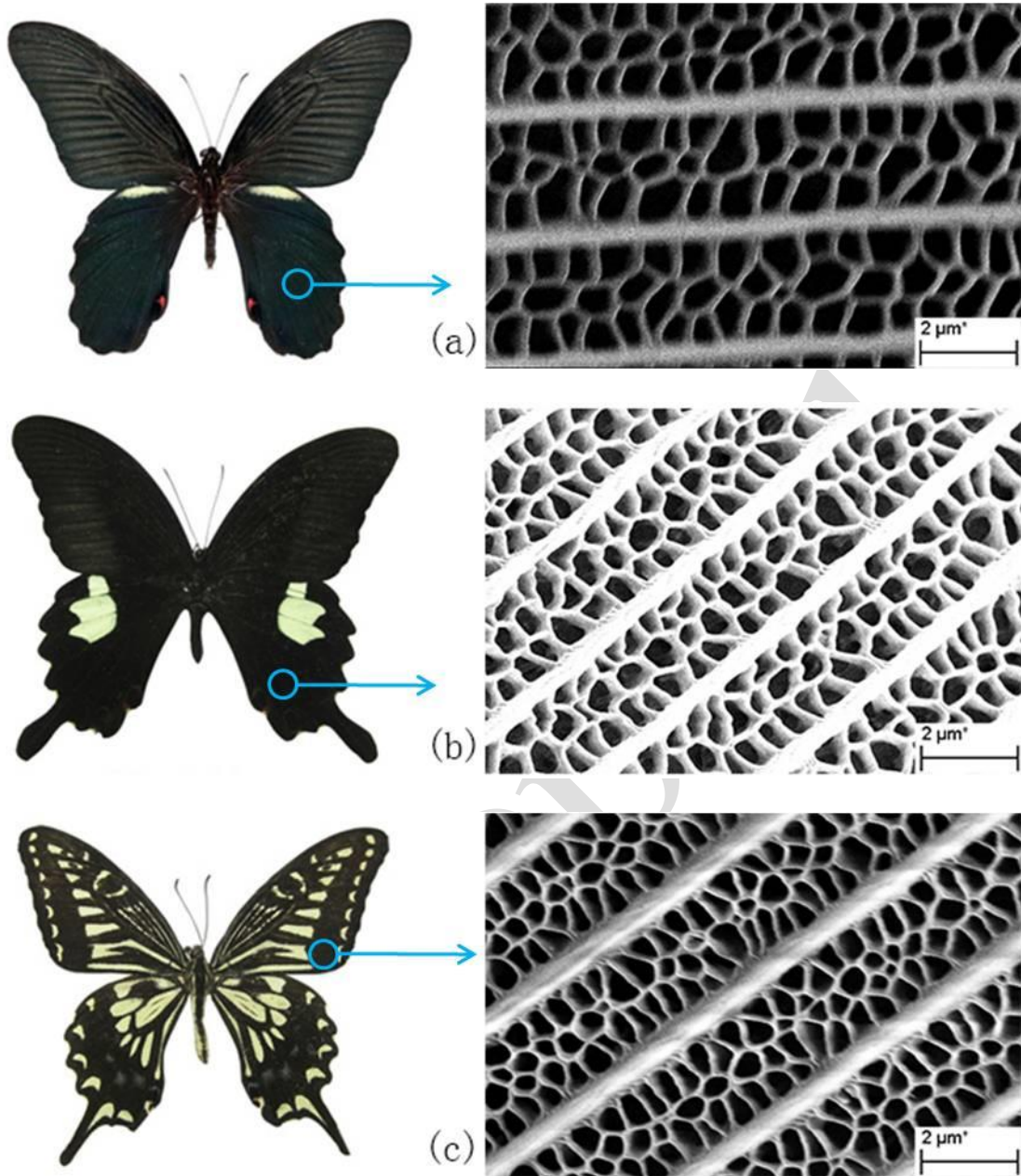
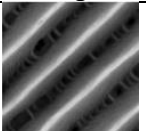
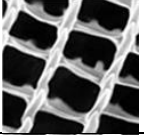
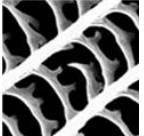
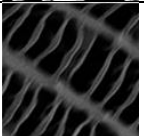
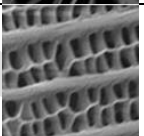
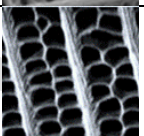
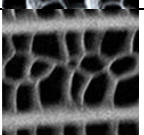
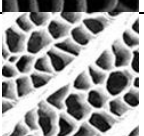
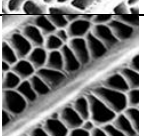


Fig. 4. The photos and SEM images of type-IV butterfly wings. (a) *Papilio protenor cramer*, (b) *Papilio helenus*, (c) *Papilio xuthus*.

The structure features of the butterfly wing scales are summarized in Table 1.

Table 1 The wing scale features of different butterfly species.

No.	Butterfly Species	Features	Featured Sizes	SEM Images
IA	Ornithoptera priamus	Type-I: V-gullies without holes	Length of the ridge bottom: 800nm Ridge separation: 200 nm	

IIA	Tirumala limniace	Type-II: V-gullies with one line of holes	Hole length: 1.7 μm Hole width: 700 nm	
IIB	Polyura athamas		Hole length: 2.0 μm Hole width: 880 nm	
IIC	Aglais io		Hole length: 2.0 μm Hole width: 600 nm	
IIIA	Graphium doson	Type-III: V-gullies with two lines of holes	Ridge periodic length: 1.75 μm Hole length & width: 800, 500 nm	
IIIB	Graphium sarpedon		Ridge periodic length: 1.5 μm Hole length & width: 700, 500 nm	
IVA	Papilio protenor cramer	Type-IV: V-gullies with three lines of holes	Ridge periodic length: 2.5 μm Holes next to a ridge: 740, 650 nm Holes in the middle line: D = 700 nm	
IVB	Papilio helenus		Ridge periodic length: 2.4 μm Holes next to a ridge: 800, 400 nm Holes in the middle line: D = 450 nm	
IVC	Papilio xuthus		Ridge periodic length: 2.5 μm Holes next to a ridge: 650, 450 nm Holes in the middle line: D = 550 nm	

3.2 Effect of microstructures on optical properties

We examined the light scattering effect of both the black and colored scales of the butterfly wings. The scattering test was shown in Fig. S1 in the supplementary material. A laser beam (650 nm) shined perpendicularly onto butterfly wing samples (IIIB and IVB). For both samples, black scales absorbed most of the light, representing high absorption property. The colored regions allowed the laser beam to pass through and showed weak scattering ability. Thus the regions with black scales are more interesting to PV applications. Optical properties of black scales of butterfly wings were quantitatively

studied under perpendicular incident light within the wavelength ranges from 300 nm to 800 nm. During optical measurements, the wing samples of *Ornithoptera priamus* (IA), *Polyura athamas* (IIB), *Graphium sarpedon* (IIIB), and *Papilio Helenus* (IVB) are measured.

Fig. 5 presents the reflectance, absorption and transmittance results of the four wing samples. In Fig. 5a, no obvious peaks are found from the reflectance spectra which is in accordance with the black appearance. The reflectance of all the four samples is very limited below 600 nm but the one of *Polyura athamas* (IIB) sample increases significantly over 600 nm and reaches 27.6% for the light of 800 nm. Although the three wing types which have hole structures present similar optical curves, the *Polyura athamas* wings (IIB) show the highest reflectance and transmittance, resulting in the lowest light absorption ability. More but smaller holes within a gully help to lower the reflectance as well as the transmittance, making larger absorption. However, among the four types of wing structures, the one without holes (*Ornithoptera priamus*, IA) shows the lowest reflectance and transmittance and thus the highest light absorption. The butterfly wing structures are thus very promising as AR coatings for Si solar cells. Despite the performance loss during structure replication, all the four types of wings show better AR performance than Si solar cells with traditional pyramid textures (~13%, Manzoor et al., 2020) or SiN_x coatings (24.86%, Ko et al., 2011).

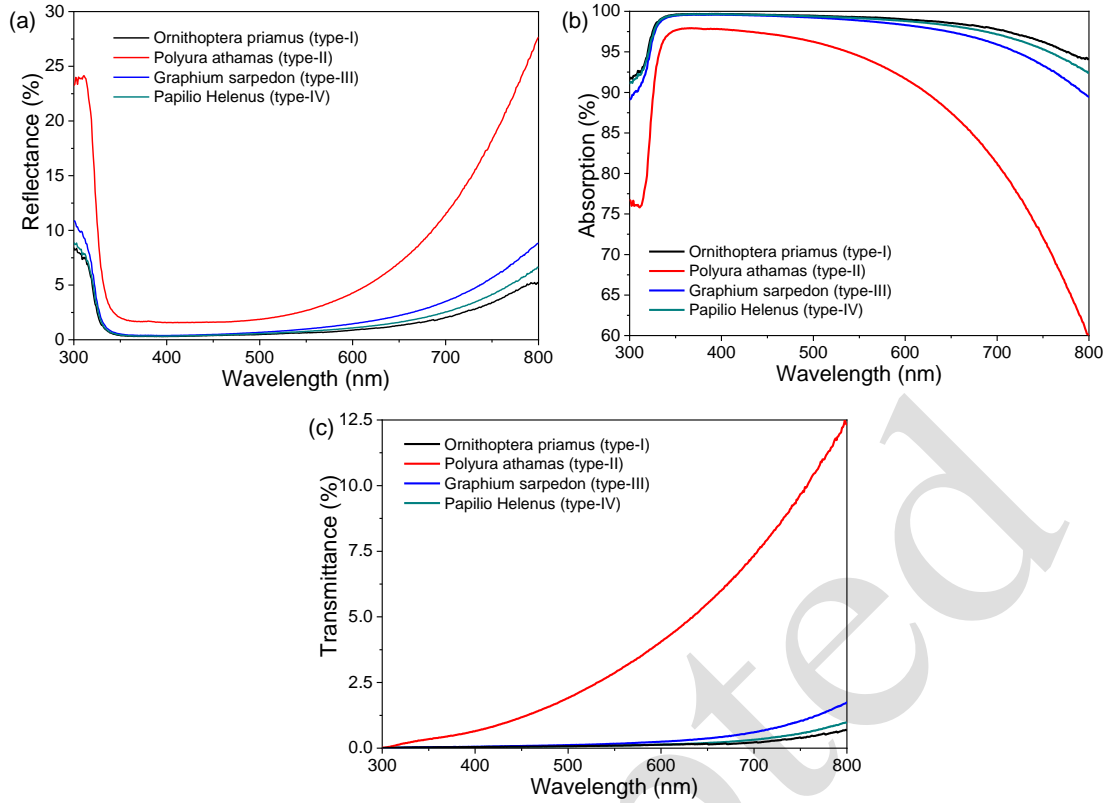


Fig. 5. Measured optical properties. (a) Reflectance, (b) Absorption, (c) Transmittance.

The optical spectra suggest possible relations between surface structures and optical performances. Especially, the gully spacing and hole arrangements show obvious influence on optical behaviors. Therefore, it is necessary to study the light-wing interactions through optical simulations. Models were constructed by using silicon material following the above four wing types which were experimentally studied: the Ornithoptera priamus (IA, Fig. 6a), Polyura athamas (IIB, Fig. 6b), Graphium sarpedon (IIIB, Fig. 6c), and Papilio Helenus (IVB, Fig. 6d). The hole shapes in each model are approximated to the SEM results. Besides the four wing models, optical performances of a flat silicon model was also computed as a reference.

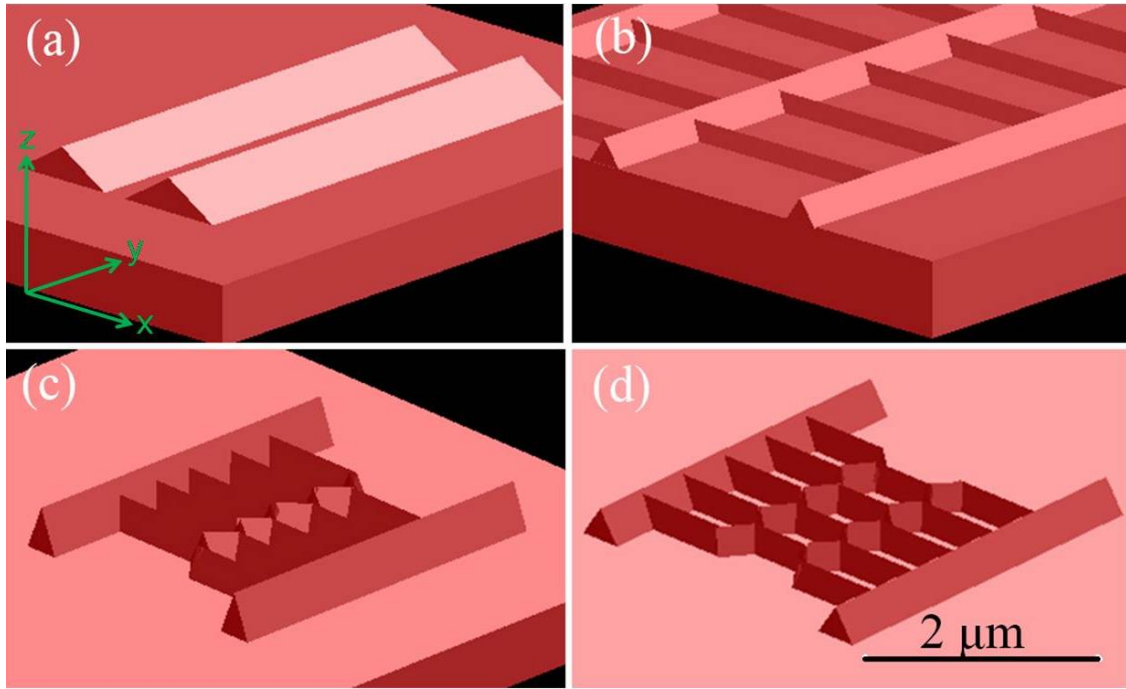


Fig. 6. Simulation models constructed following the wing scales of (a) type-I, (b) type-II, (c) type-III, and (d) type-IV.

The simulated optical spectra are presented in Fig. 7. Among the five models including the bare Si, the flat silicon model has the highest reflectance and the spectrum agrees well with previous reports (Huang et al., 2018) (Fig. 7a). More than 30% of the light is reflected which limits the photovoltaic efficiency of silicon-based solar cells. Introducing gullies and holes on silicon surface obviously decreases the light reflection. The model with only gullies (type-I) has the lowest reflectance which is less than 10% within the whole wavelength range of visible light. Involving holes within gullies increases reflectance values, however, such reflectance promotion could be prohibited by enlarging the hole amounts and squeezing the hole sizes. Thus the type-IV model shows lowest reflectance among the three models with holes. Such reflectance spectra are in consistent with the experimental results. As for the absorption properties (Fig. 7b), the

type-I model shows the best light absorption ability. More than 70% of the visible light is absorbed. Holes on the silicon surface weaken light absorption where the type-IV model has relatively larger absorption ability than the other two models with holes. Flat silicon model gives the lowest absorption ability for visible light. The above results suggest that one model that has lower reflection always presents higher optical absorption. The simulated transmittance spectra are slightly deviated from the experimental results (Fig. 7c). The *Ornithoptera priamus* model (type-I) still shows the lowest transmittance, but the *Graphium sarpedon* model (type-III) gives the highest transmittance. The spectra of the other three models are very close. Such deviation may be caused by the different materials between the butterfly wings and the models. The wings are mainly composed of organic compounds and pigments while the models are constructed by silicon material. It is noteworthy that the experimental results were collected on bare wings which were covered by the multilayers of scales. Interlayer interferences of light also count for the overall color performances on the scales (Dumanlia and Savin 2016) but were not considered in the simplified models. Despite the small deviation in optical transmittance, the simulation results agree well with experimental data. It suggests that the models are well constructed so that further exploration of these models is possible.

Based on the experimental and simulated results, it is very exciting that the butterfly wings are endowed with very low reflectance. For IA, IIIB and IVB wings, the reflectance is below 2.5% in the wavelength range of 350 – 700 nm. When the wing structures are transferred on Si slabs, the upside reflectance is still very low, especially for the IA

structure (below 10% in the whole range of visible light). Such reflection suppression is attributed to the periodic ridges whose characteristic sizes are comparable to the wavelength of visible light (Sayigh 2012). In addition, wing structures also enhance the light absorption in the whole visible wavelength range. A careful look at the scale shows that the main frame owns a triangle prism structure, different from the rods in other types of IIIB and IVB. Such a prism can be visualized as the connected pyramids which are very beneficial to the light harvesting according to the biomimic studies using foliage as the masters (Huang et al., 2015; Huang et al., 2016). We also noticed that structures of IA may benefit from good antireflection and light trapping properties of the wing structures in long wavelength region and grating effect of periodically arranged ridges in short wavelength region (Chong et al., 2012; Fonash et al., 2014).

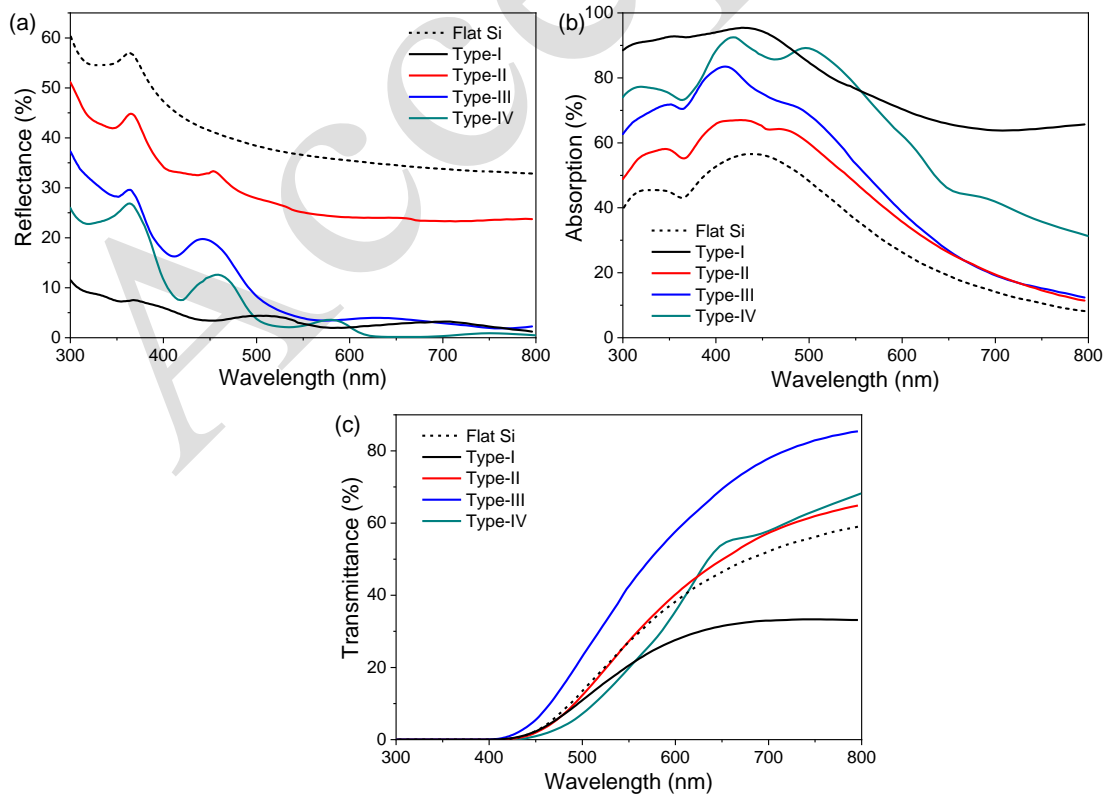


Fig. 7. Simulated optical properties. (a) Reflectance, (b) Absorption, (c) Transmittance.

It should be mentioned that the thickness of Si slabs in the simulation is much smaller than commercial solar cell wafers. According to the 2019 report of International Technology Roadmap for Photovoltaic (ITRPV), the minimum thickness of silicon wafers is around 170 ~ 180 μm . Current computational hardware cannot afford such a thickness. The Si slab thickness is 1.2 μm in this paper. We found that increasing slab thickness reduced the transmittance but the reflectance kept stable, see Fig. S2 in Supplementary material.

Based on the above models, short currents were calculated to evaluate the photo-to-current efficiency. The short current here is photocurrent. The short current values of the flat silicon model and the four wing models are listed in Table 2. Not surprisingly, the type-I model gives the best photocurrent performance (13.48 mA/cm^2) and the flat silicon model the worst (8.12 mA/cm^2). There is a 66% increase of current density without considering surface recombination. With an optimized surface structures, the current density could be enhanced by more than 100% (Chong et al., 2012). However, such enhancement is hard to achieve in real case (Da and Xuan 2013). Among the three models with both gullies and holes, more but smaller holes filled within a gully (the type-IV model) leads to better photocurrent performance. The photo-to-current property is more clearly visualized by light trapping (Fig. 8). Regions in red have better light trapping ability than the other regions. Flat silicon model shows the lowest light-trapping ability due to its high reflectance of visible light. Wing structures including the gullies and holes on the models facilitate light trapping and the type-I model with only gullies turned out

to be the best candidate for light trapping.

Table 2. Calculated short current values of the flat Si model and four wing models.

Samples	Flat Si	Type-I	Type-II	Type-III	Type-IV
Short current $J_{sc}(\text{mA}/\text{cm}^2)$	8.12	13.48	8.63	10.45	11.05

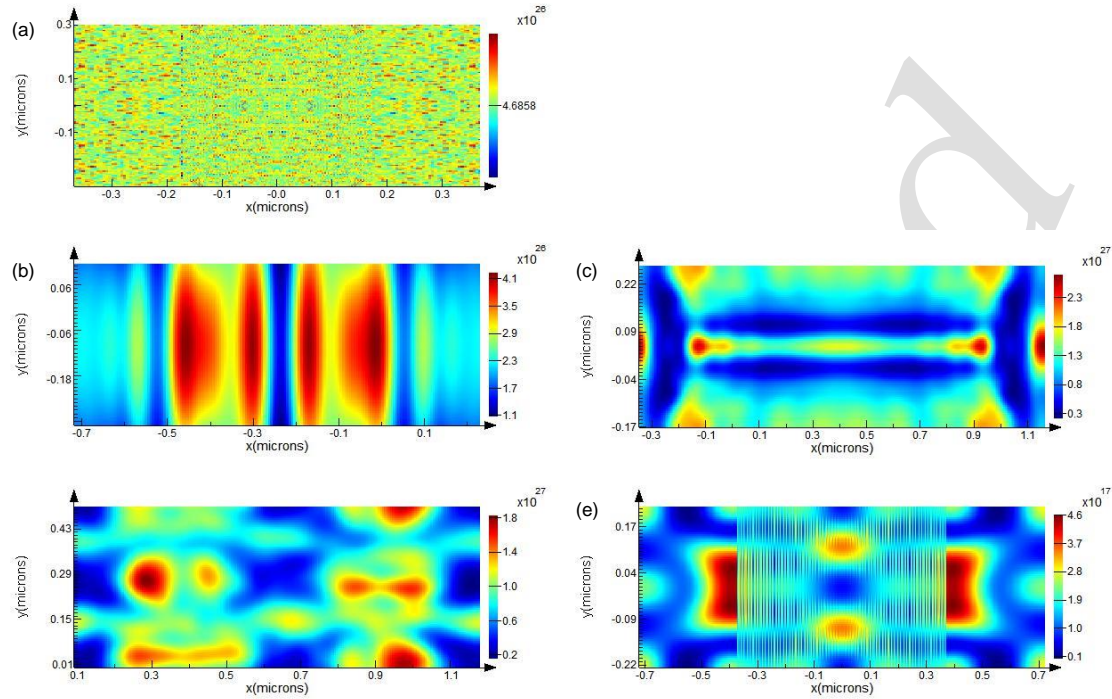


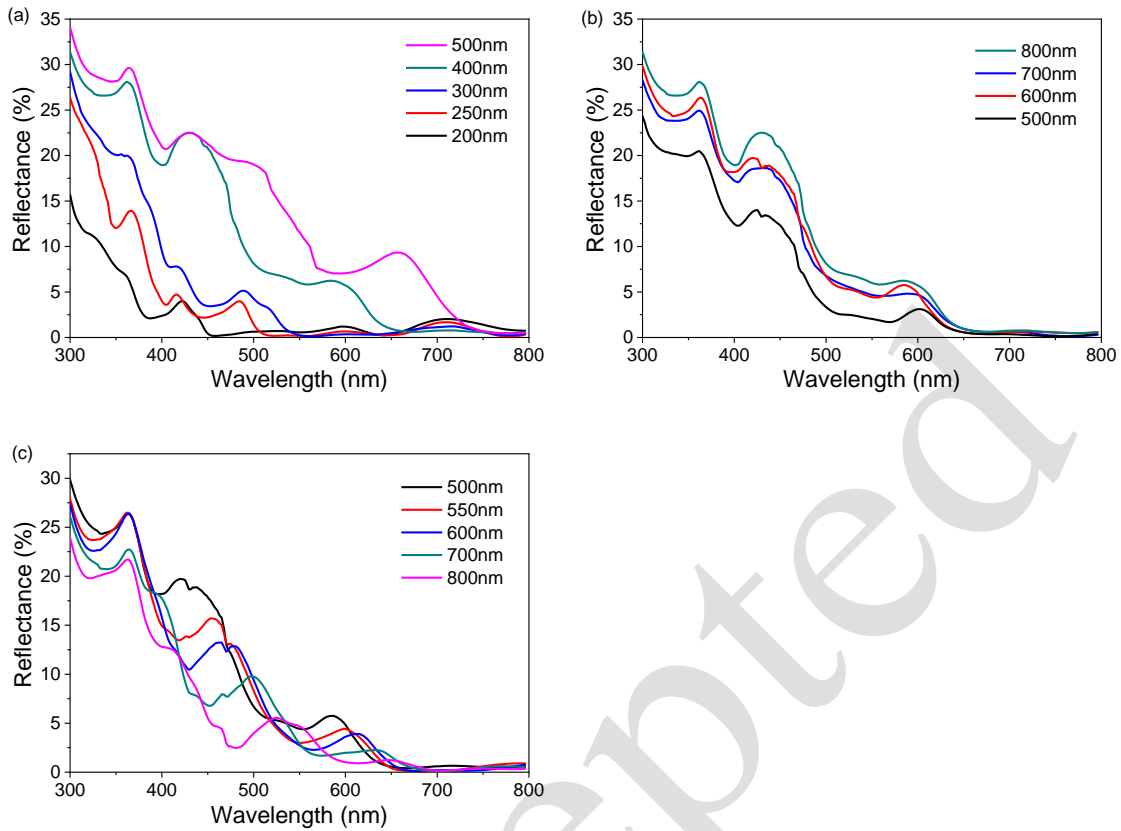
Fig. 8. Light-trapping mappings of (a) flat silicon model, (b) type-I model, (c) type-II model, (d) type-III model, and (e) type-IV model.

Considering both experimental and calculated optical properties, it is obvious that replicating surface structures of the black regions of butterfly wings on silicon lowers the reflectance and transmittance of visible light and thus improves the light absorption. Pure gullies introduced on top of flat silicon lead to the best light trapping ability. Putting holes within gullies hinders the light absorption, however, such negative effect could be alleviated by increasing the amount and decreasing the size of holes within one gully.

3.3 Effect of hole parameters on optical properties

Since the hole structures play a significant role on optical properties, it is necessary to investigate how do the sizes of holes affect optical performances. Besides, hole sizes are also different among the butterfly wings (type-II, III, IV). In this case, we further studied the effect of hole sizes on reflectance based on the type-III model. Fig. 9a shows that the reflectance changes due to the variations of hole widths. The reflectance drops when the hole widths decrease from 500 nm to 200 nm. The same behavior appears when adjusting the hole lengths from 800 nm to 500 nm (Fig. 9b). The hole depths are also studied in Fig. 9c. It shows that the reflectance slightly reduces with deeper holes below the wavelength of 500 nm. The influence of hole depths is quite limited over the wavelength of 500 nm. Such results suggest that smaller widths or lengths of the holes facilitate the weakening of visible light reflectance, and that lateral sizes of holes have more obvious influences on reflectance compared with hole depths. The reflection process could be visualized by the light propagations (Chong et al., 2012). We designed several structures of different lateral and vertical sizes and arranged them in one model. The animations of light propagation were provided by Supplementary videos. Snap shots of photon paths were shown in Fig. S3 and Fig. S4. It can be seen that the reflection of smaller vertical structures is stronger compared with those of larger depth. On the other hand, structures squeezed in lateral dimensions lead to more obvious reflection. But the reason why lateral sizes have greater effect on reflection compared to vertical sizes still need further investigation.

335



336

337

338 Fig. 9. The influence of hole parameters on reflectance at normal incidence. (a) Hole
 339 widths. (b) Hole lengths. (c) Hole depths.

340 3.4 Applicability to solar cells

341 The optical performance of butterfly wing structures is promising to improve the
 342 efficiency of solar cells. For industrial applications, such bio-mimicked structures should
 343 be able to reduce reflectance for any incident angle. Besides the circumstance of normal
 344 incidence in Fig. 7, the reflectance at a 30° incident angle was calculated and shown in
 345 Fig. 10. Compared to flat silicon model, the butterfly wing structures always reduces the
 346 reflectance. It suggests that the structures of butterfly wing scales have good adaptability
 347 to natural light incidence which makes them applicable for capturing daylight of various

348 incident angles.

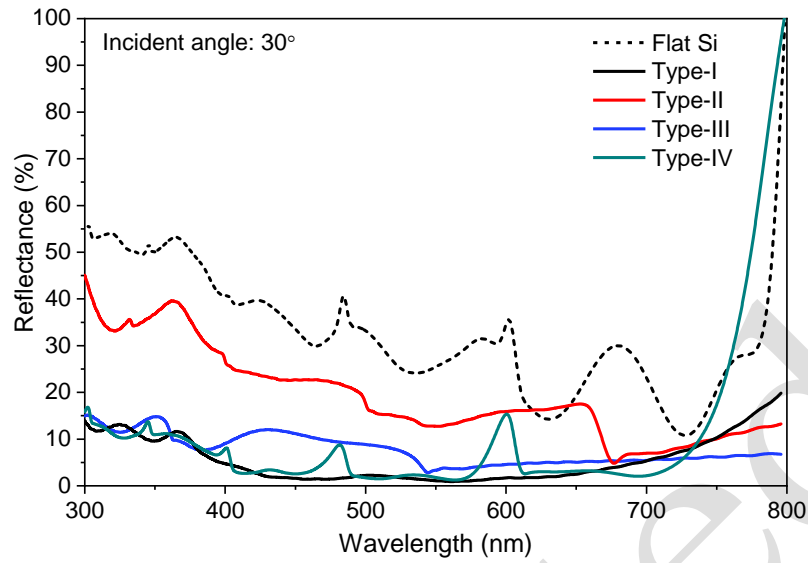


Fig. 10. Simulated reflectance for 30° incidence.

The type-I structure gives the lowest reflectance for both perpendicular and oblique incidence. Such wing structure is featured with V-shape gullies without holes. With a ridge bottom of 800 nm and ridge interval of 1 μm , it is available to be replicated with polydimethylsiloxane (PDMS) through a soft lithography method (Kang et al., 2010). The PDMS replica is easy to be transferred on silicon surface and it can keep both the microstructural and optical characteristics of butterfly wings. Such preparation process is quite straightforward and viable for mass production. However, the wing structures of type-II, III and IV are much more complicated due to the polygonal holes between ridges. Replicating such wing structures involves multi-steps of masking and etching. It is thus challenging for industrial production. Moreover, when applied to silicon solar cells, the replica of wing structures will increase surface recombination (Da and Xuan 2013). In this case, surface passivation is necessary to mitigate such problem (Schmidt et al., 2018).

Among current techniques, applying dielectric layers through remote plasma enhanced chemical vapor deposition (PECVD) is typically used for rear side passivation, and phosphorous or boron doping is often used for front side passivation (Bonilla et al., 2017; Allen et al., 2019). Both of them may be applicable in the case of an organic bio-replica layer. The latest work by using a heat-shrinking printing method showed that direct patterning and integration of color specified species are applicable in realizing the 3D photonic structures onto a wide scope of matrixes (Liu et al., 2019).

4. Conclusions

In conclusion, a biomimicry antireflection strategy has been realized on Si-based solar cells. Different from most bio-inspired routes using the foliage as master, the present route show that microstructures on animals also benefit light harvesting. Through experimental and computational methods, we find that introducing wing structures on flat silicon surface facilitates the reduction of visible light reflectance and thus promotes light trapping. Gully structures improve the light absorption best, and hole structures are also useful in case that they are controlled in relatively small sizes. Such findings are useful for the design and development of optical devices especially those utilized for solar cells.

Declaration of Competing Interest

None.

Acknowledgements

The authors acknowledge the financial supports from the Academy of Finland (No. 311934), the National Natural Science Foundation of China (No. 61904069), and funding

from Anhui Polytechnic University (No. 2016BJRC005) and the Natural Science Foundation of Jiangsu Higher Education Institutions of China (No.19KJB140008). W.C. thanks the Anhui Provincial Grant for high-level platform construction. The Center of Microscopy and Nanotechnology of the University of Oulu is acknowledged for sample characterizations. Dr. Hui Zhang at Soochow University is acknowledged for FDTD simulation.

Appendix A. Supplementary material

Supplementary data associated with this article can be found, in the online version.

References

- Allen, T.G., Bullock, J., Yang, X., Javey, A., Wolf, S.D., 2019. Passivating contacts for crystalline silicon solar cells. *Nat. Energy* 4, 914–928.
- Bonilla, R.S., Hoex, B., Hamer, P., Wilshaw, P.R., 2017. Dielectric surface passivation for silicon solar cells: A review. *Phys. Status Solidi A* 214, 1700293.
- Chong, T.K., Wilson, J., Mokkaapati, S., Catchpole, K.R., 2012. Optimal wavelength scale diffraction gratings for light trapping in solar cells. *J. Opt.* 14, 024012.
- Conibeer, G., Green, M., Corkish, R., Cho, Y., Cho, E.C., Jiang, C.W., Fangsuwannarak, T., Pink, E., Huang, Y., Puzzer, T., Trupke, T., 2006. Silicon nanostructures for third generation photovoltaic solar cells. *Thin Solid Films* 511, 654–662.
- Da, Y., Xuan, Y., 2013. Role of surface recombination in affecting the efficiency of nanostructured thin-film solar cells. *Opt. Express* 21, A1065–A1077.
- Duan, Z., Li, M., Trevor, M.C., 2018. Effective light absorption using the double-sided pyramid gratings for thin-film silicon solar cell. *Nanoscale Res. Lett.* 13, 192.
- Dullweber, T., Hesse, R., Bhosle, V., Dubé, C., 2013. Ion-implanted PERC solar cells with $\text{Al}_2\text{O}_3/\text{SiN}_x$ rear passivation. *Energy Procedia* 38, 430–435.
- Dumanli, A.G., Savin, T., 2016. Recent advances in the biomimicry of structural colours. *Chem. Soc. Rev.* 45, 6698–6724.
- Fonash, S.J., 2014. *Introduction to Light Trapping in Solar Cell and Photo-detector Devices*. Academic Press.
- Fujishima, D., Kanno, H., Kinoshita, T., Maruyama, E., Tanaka, M., Shirakawa, M., Shibata, K., 2009. Organic thin-film solar cell employing a novel electron-donor material. *Sol. Energy Mater. Sol. Cells* 93, 1029–1032.
- Han, Z., Niu, S., Shang, C., Liu, Z., Ren, L., 2012. Light trapping structures in wing scales of butterfly trogonoptera brookiana. *Nanoscale* 4, 2879–2883.

417 Hofstetter, J., del Canizo, C., Ponce-Alcantara, S., Luque, A., 2007. Optimisation of
 418 SiNx:H anti-reflection coatings for silicon solar cells. Spanish Conference on
 419 Electron Devices, IEEE, 131–134.

420 Hong, S., Bae, J., Koo, B., Chang, I., Cho, G.Y., Kim, Y.-B., Cha, S.W., Prinz, F.B., 2014.
 421 Nanostructuring methods for enhancing light absorption rate of Si-based
 422 photovoltaic devices: A review. *International Journal of Precision Engineering and*
 423 *Manufacturing-Green Technology* 1, 67–74.

424 Huang, Z., Yang, S., Zhang, H., Zhang, M., Cao, W., 2015. Replication of leaf surface
 425 structures for light harvesting. *Sci. Rep.* 5, 14281.

426 Huang, Z., Shi, T., Zhang, H., Zhang, M., Huttula, M., Cao, W., 2016. A computational
 427 study of antireflection structures bio-mimicked from leaf surface morphologies. *Sol.*
 428 *Energy* 131, 131–137.

429 Huang, Z., Cai, C., Kuai, L., Li, T., Huttula, M., Cao, W., 2018. Leaf-structure patterning
 430 for antireflective and self-cleaning surfaces on Si-based solar cells. *Sol. Energy* 159,
 431 733–741.

432 Ikhmayies, S., 2018. *Advances in Silicon Solar Cells*. Springer International Publishing
 433 AG.

434 Ju, M., Balaji, N., Park, C., Nguyen, H.T.T., Cui, J., Oh, D., Jeon, M., Kang, J., Shim, G.,
 435 Yi, J., 2016. The effect of small pyramid texturing on the enhanced passivation and
 436 efficiency of single c-Si solar cells. *RSC Adv.* 6, 49831.

437 Kang, S.-H., Tai, T.-Y., Fang, T.-H., 2010. Replication of butterfly wing microstructures
 438 using molding lithography. *Current Appl. Phys.* 10, 625–630.

439 Ko, J., Gong, D., Pillai, K., Lee, K.S., Ju, M., Choi, P., Kim, K.R., Yi, J., Choi, B., 2011.
 440 Double layer SiNx:H films for passivation and anti-reflection coating of c-Si solar
 441 cells. *Thin Solid Films* 519, 6887–6891.

442 Lelièvre, J.F., Kafle, B., Saint-Cast, P., Brunet, P., Magnan, R., Hernandez, E., Pouliquen,
 443 S., Massines, F., 2019. Efficient silicon nitride SiNx:H antireflective and passivation
 444 layers deposited by atmospheric pressure PECVD for silicon solar cells. *Prog.*
 445 *Photovolt. Res. Appl.* 27, 1007–1019.

446 Lewis, N.S., 2016. Research opportunities to advance solar energy utilization. *Science*
 447 351, 353.

448 Li, Y., Zhang, Y., Lin, J., Fang, C., Ke, Y., Tao, H., Wang, W., Zhao, X., Li, Z., Lin, Z.,
 449 2018. Multiscale array antireflective coatings for improving efficiencies of solar
 450 cells. *Appl. Surf. Sci.* 462, 105–111.

451 Li, W., Tan, X., Zhu, J., Xiang, P., Xiao, T., Tian, L., Yang, A., Wang, M., Chen, X., 2019.
 452 Broadband antireflective and superhydrophobic coatings for solar cells. *Mater.*
 453 *Today Energy* 12, 348–355.

454 Liu, D., Yu, H., Duan, Y., Li, Q., Xuan, Y., 2016. New insight into the angle insensitivity
 455 of ultrathin planar optical absorbers for broadband solar energy harvesting. *Sci. Rep.*
 456 6, 32515.

457 Liu, Y., Wang, H., Ho, J., Ng, R.C., Ng, R.J.H., Hall-Chen, V.H., Koay, E.H.H., Dong, Z.,
 458 Liu, H., Qiu, C.W., Greer, J.R., Yang, J.K.W., 2019. Structural color three-

dimensional printing by shrinking photonic crystals. *Nat. Commun.* 10, 4340.

Manzoor, S., Filipič, M., Onno, A., Topič, M., Holman, Z.C., 2020. Visualizing light trapping within textured silicon solar cells. *J. Appl. Phys.* 127, 063104.

Paudel, N.R., Yan, Y., 2013. Fabrication and characterization of high-efficiency CdTe-based thin-film solar cells on commercial SnO₂:F-coated soda-lime glass substrates. *Thin Solid Films* 549, 30–35.

Savin, H., Repo, P., von Gastrow, G., Ortega, P., Calle, E., Garín, M., Alcubilla, R., 2015. Black silicon solar cells with interdigitated back-contacts achieve 22.1% efficiency. *Nat. Nanotech.* 10, 624–628.

Sayigh, A., 2012. *Comprehensive Renewable Energy*, 1st Edition. Elsevier Ltd.

Schmidt, J., Aberle, A.G., 1999. Carrier recombination at silicon–silicon nitride interfaces fabricated by plasma-enhanced chemical vapor deposition. *J. Appl. Phys.* 85, 3626–3633.

Schmidt, J., Werner, F., Veith, B., Zielke, D., Steingrube, S., Altermatt, P.P., Gatz, S., Dullweber, T., Brendel, R., 2012. Advances in the surface passivation of silicon solar cells. *Energy Procedia* 15, 30–39.

Schmidt, J., Peibst, R., Brendel, R., 2018. Surface passivation of crystalline silicon solar cells: Present and future. *Sol. Energy Mater. Sol. Cells* 187, 39–54.

Shi, X., Huang, Z., Laakso, M.J., Niklaus, F., Sliz, R., Fabritius, T., Somani, M., Nyo, T., Wang, X., Zhang, M., Wang, G., Kömi, J., Huttula, M., Cao, W., 2019. Quantitative assessment of structural and compositional colors induced by femtosecond laser: A case study on 301LN stainless steel surface. *Appl. Surf. Sci.* 484, 655–662.

Siddique, R.H., Donie, Y.J., Gomard, G., Yalamanchili, S., Merdzhanova, T., Lemmer, U., Hölscher, H., 2017. Bioinspired phase-separated disordered nanostructures for thin photovoltaic absorbers. *Science* 3, e1700232.

Sopori, B.L., Madjdpour, J., Chen, W., Zhang, Y., 1999. Light-Trapping in a-Si Solar Cells: A Summary of the Results from PV Optics. *AIP Conference Proceedings* 462, 291–296.

Wasserthal, L.T., 1975. The role of butterfly wings in regulation of body temperature. *J. Insect Physiol.* 21, 1921–1930.

Wu, X., Zhang, Z., Liu, Y., Chu, X., Li, Y., 2015. Process parameter selection study on SiNx:H films by PECVD method for silicon solar cells. *Sol. Energy* 111, 277–297.

Yue, Z., Shen, H., Jiang, Y., 2013. Antireflective nanostructures fabricated by reactive ion etching method on pyramid-structured silicon surface. *Appl. Surf. Sci.* 271, 402–406.

Zhan, Y., Wang, Y., Cheng, Q., Li, C., Li, K., Li, H., Peng, J., Lu, B., Wang, Y., Song, Y., Jiang, L., Li, M., 2019. A butterfly-inspired hierarchical light-trapping structure towards a high-performance polarization-sensitive perovskite photodetector. *Angew. Chem., Int. Ed.* 58, 16456–16462.